Ab initio studies on the structural and dynamical properties of ice

Changyol Lee*

Department of Physics, Harvard University, Cambridge, Massachusetts 02138

David Vanderbilt

Department of Physics and Astronomy, Rutgers University, Piscataway, New Jersey 08855-0849

Kari Laasonen[†]

Institut Romand de Recherche Numérique en Physique des Matériaux, PHB-Ecublens, CH-1015 Lausanne, Switzerland

R. Car

*Institut Romand de Recherche Numerique en Physique des Matériaux, PHB-Ecublens, CH-1015 Lausanne, Switzerland
and Department of Condensed Matter Physics, University of Geneva, Geneva, CH-1211, Switzerland*

M. Parrinello

IBM Research Division, Zürich Research Laboratory, CH-8803 Rüschlikon, Switzerland

(Received 28 September 1992)

The structural and dynamical properties of cubic H_2O and D_2O ice phases are studied using *ab initio* molecular dynamics combined with ultrasoft pseudopotentials. Phonon frequencies are extracted from the velocity autocorrelation functions; contributions from different normal modes in the phonon spectra are separated and easily identified. For the low-pressure phases, the agreement with the experimental data is reasonable and the isotope effects are well reproduced. High-pressure phases are also studied. The equations of state for cubic ice (ice I_c), and for the ice VII-VIII-X family, are calculated. It is found that the local-density approximation must be augmented with gradient corrections in order to obtain a proper description of the hydrogen bond. Finally, the hydrogen-bond symmetrization, which is responsible for the transition from ice VII-VIII to ice X, is studied and is predicted to occur at 49 GPa. The nature of the phase transition is found to be that of a mode-softening transition. The corresponding symmetrization is also studied in ice I_c, but it is found to occur at a pressure of 7 GPa at which ice I_c is unstable with respect to denser phases.

I. INTRODUCTION

The physical and chemical properties of water are of obvious interest, and have led to a huge number of theoretical studies using semiempirical methods. However, advances in computational methodology and computer power hold the promise of a new generation of studies using *ab initio* quantum-mechanical approaches. *Ab initio* quantum-chemical methods have already been applied to water molecules and dimers[1−4] and even trimers[5] and small clusters.[6] But the most promising approach for the study of larger aggregates, including crystalline ice and liquid water phases, is likely to be the density-functional theory (DFT).[7] To date, density-functional calculations on H_2O systems have been limited to molecules and dimers,[8,9] but there is no fundamental obstacle to the application of these methods to larger systems. Moreover, the introduction of the *ab initio* molecular dynamics by Car and Parrinello (CP) (Ref. 10) opens the possibility of efficient studies of dynamical properties, in addition to the calculation of static energetics.

Two technical problems have hindered the widespread application of DFT methods to H_2O systems. First, the preferred approach (especially for dynamical studies) has been the plane-wave pseudopotential approach, in which forces on atoms can be calculated in a straightforward manner. However, the description of first-row atoms like oxygen is problematic in plane-wave schemes, because of the very large number of plane-wave components needed to describe the rather localized oxygen $2p$ orbitals. Second, because there have been relatively few DFT calculations on hydrogen-bonded systems, the accuracy of the local-density approximation (LDA) (Ref. 11) for this class of systems is not well established. After all, the Van der Waals interaction, which is another (but weaker) form of attractive interaction between closed-shell systems, is known to be poorly described within LDA.

In this paper we adopt the "ultrasoft" pseudopotentials recently introduced by Vanderbilt,[12] which offer a very smooth and high-quality description of the oxygen atom and other first-row and transition-metal elements. Moreover, we augment the LDA with gradient corrections,[13,14] and confirm that this leads to an accurate description of the intermolecular interaction. These adaptions allow us to study the properties of H_2O and D_2O systems within DFT, using both static energetic and CP molecular-dynamics calculations, at a modest computational cost.

As the structure of the solid state is generally more easily described than that of the corresponding liquid, we

have decided to focus here on crystalline ice phases. There has been considerable experimental work to identify the various structural modifications of ice, stable or metastable under a variety of conditions, and to elucidate the structures and vibrational signatures of these polymorphs.[15] Here we investigate the structural and dynamical properties of several ice phases with cubic symmetry. In particular, the phonon densities of states of (low-pressure) H_2O and D_2O ice I_c at low temperature are calculated from first principles and compared with experiment. The contributions from the different normal modes in the phonon spectra are separated and easily identified. The isotope shifts associated with the replacement of protons by deuterons are well reproduced. Also, the equations of state for ice I_c and the ice VII-VIII-X system have been calculated. A good description of the intermolecular interaction is obtained only after gradient corrections to LDA are included. The phase transitions into symmetric hydrogen-bonded ice at low pressure (ice I_c) and high pressure (ice VII-VIII→X) are studied, and identified as mode-softening transitions.

This article is organized as follows: In Sec. II, the experimental background on ice is reviewed. Section III briefly discusses our theoretical method. In Sec. IV, the results from the *ab initio* molecular-dynamics calculations on cubic ice and ice X are presented, and Sec. V presents a summary and conclusion. The appendix presents a brief discussion of the physical interpretation of the velocity autocorrelation function.

II. EXPERIMENTAL BACKGROUND

Ordinary hexagonal ice (ice I_h) is obtained when liquid water freezes at atmospheric pressure. Roughly speaking, the oxygen atoms in ice I_h comprise a wurtzite lattice (the hexagonal modification of the diamond lattice), while hydrogen atoms occupy asymmetric sites along the O–O bonds and are disordered within the Pauling ice rules[16] (i.e., each O atom has two nearer and two further H neighbors). This ice disorder persists down to 0 K. There is a modification of ice I_h, referred to as cubic ice or ice I_c, which is similar except that the oxygen atoms comprise a diamond lattice. Ice I_c cannot be obtained by cooling ice I_h, but can be obtained by the condensation of water vapor below $-80\,°C$. Ice I_c is metastable between -80 and $-120\,°C$, at which temperature it becomes stable. The structure of ice I_c is shown in Fig. 1. The hydrogen atoms are also disordered within the Pauling ice rules in ice I_c.

The vibrations of ice I_h and ice I_c crystals have been extensively studied using infrared[17-21] and Raman[17,22-24] spectroscopy, and have been the subject of theoretical calculations.[25,26] Spectroscopic studies on ice I_h and ice I_c have shown that there is no substantial difference in their infrared[18] and Raman[23,24] spectra. This is not surprising because ice I_h and I_c have the same nearest-neighbor bonding configuration and the same number of next-nearest neighbors. (The prominent features of the spectra from the experiments are summarized in Table II.) The assignment of observed spectral peaks to individual modes has been greatly facilitated by
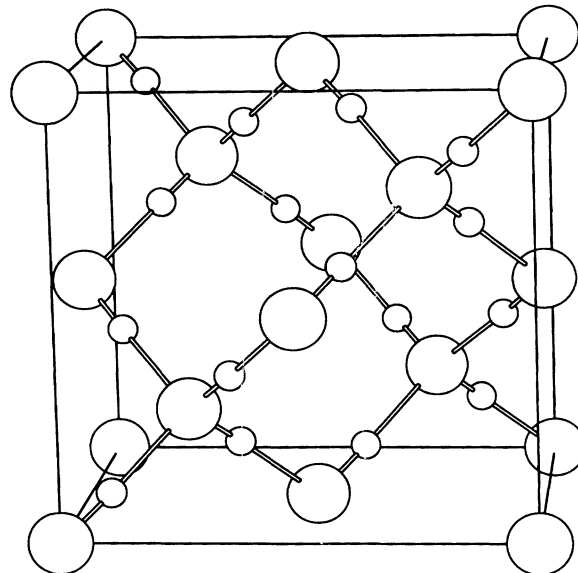

FIG. 1. Structure of ice I_c. The unit cell has eight H_2O molecules with oxygen atoms denoted by bigger circles and hydrogen atoms by smaller circles.

comparison of spectra of protonated and deuterated ice, so that a fairly complete analysis is possible. In this article, we calculate the phonon densities of states of H_2O and D_2O ice from first principles and identify contributions from the individual normal modes.

Since the stable form of a material is determined by the condition that the Gibbs free energy is a minimum at a specified temperature and pressure, the structures with the lowest volume are preferred when the pressure is high. For the case of ice, more and more close-packed structures are generated as the pressure is increased up to a few tens of GPa. However, all forms from ice I to ice IX have intact water molecules as their basic building blocks. The moderately high-pressure ice VII and VIII phases, for example, can be thought of as consisting of two interpenetrating I_c structures, as shown in Fig. 2. (In the cubic ice VII structure, the protons are again disordered within the Pauling ice rules. In ice VIII, on the other hand, the two sublattices are fully ordered and oppositely polarized, resulting in an antiferroelectric structure that is almost cubic but with a small tetragonal distortion.) In these phases, it is known that the covalently bonded O–H distance *increases* with increasing pressure, while the hydrogen-bonded O–O distance naturally decreases.[27] At a sufficient high pressure, the molecular picture is expected to break down entirely, and the hydrogens should reside at the midpoint of the O–O bonds. Such a speculative phase has been designated ice X.

There has been some experimental evidence suggesting a transition into ice X. Hirsch and Holzapfel[28] found a new band above 40 GPa in the Raman spectra of ice VIII up to 50 GPa at 100 K. Polian and Grimsditch[29] observed an anomaly in the behavior of the longitudinal sound velocity at 44 GPa from Brillouin scattering stud-
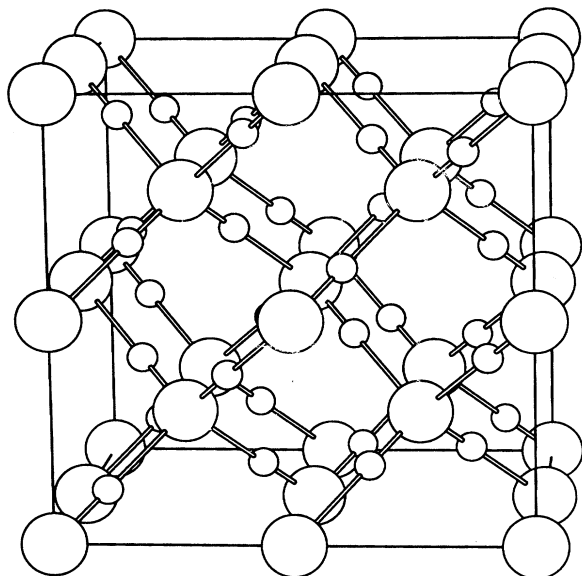
FIG. 2. Structure of ice VIII. The unit cell has 16 H_2O molecules with oxygen atoms denoted by bigger circles and hydrogen atoms by smaller circles. The ice X structure would be obtained by displacing all the hydrogen atoms into O–O bond midpoints. The small tetragonal distortion of ice VIII is not shown.

ies up to 67 GPa. Walrafen *et al.*[30] also suggested that a symmetric hydrogen-bond structure might form in ice VII at pressures of about 75 ± 20 GPa by extrapolating Raman spectra from lower pressures. However, these experiments have left many questions unanswered. They could not distinguish the order of the transition (first order vs second order), nor did they provide useful information about the structure of the high-pressure phase. Thus, the nature of the transition has been entirely speculative.

Theoretically, studies based on empirical interatomic potentials have supported the notion of a transition to the ice X structure. An early theoretical calculation by Holzapfel[31] predicted a transition to symmetric hydrogen bonding in ice VII at pressures between 35 and 80 GPa. The interaction of the hydrogen atoms with the two nearest-neighbor oxygen atoms was approximated by equivalent Morse potentials. Later, a calculation by Stillinger and Schweizer[32] predicted a transition at roughly 60 GPa. This work included a treatment of the quantum-mechanical many-body problem for coupled proton motions along hydrogen bonds. A more recent estimate by the same authors[33] puts the transition at about 45 GPa. Also, Stillinger and Schweizer[32] suggested that the symmetrization of the hydrogen bond could be achieved in ice I_c at some high pressure which is much lower than that for ice VII-VIII. However, the accuracy and applicability of these semiempirical approaches remains questionable, and it is clear that *ab initio* calculations have an important role to play in clarifying the situation.

III. THEORETICAL METHOD

Our theoretical method consists of the *ab initio* molecular-dynamics approach proposed by Car and Parrinello[10] combined with the ultrasoft pseudopotentials introduced by Vanderbilt.[12] As discussed in the introduction, the latter allow for an efficient plane-wave representation of the localized valence orbitals associated with first-row and transition-metal elements. A review of the Vanderbilt pseudopotential formalism and some additional details of the pseudopotential generation procedure are given in Ref. 34. The pseudopotential for oxygen is generated in the neutral ground-state configuration, with a cutoff radius of 1.5 a.u. for the valence electronic wave functions and 1.2 a.u. for the local potential. Two reference energies at -1.76 and -0.67 Ry (corresponding to the s and p eigenvalues) are used for both the s and p channels in the nonlocal potential. Previous tests have demonstrated that the Vanderbilt pseudopotentials generated with these parameters provide a very smooth and accurate description of oxygen atoms.[35] For the case of hydrogen, also generated in the neutral ground-state configuration, the cutoff radii for the valence electronic wave function and the local potential are 0.8 and 0.6 a.u., respectively. One reference energy at -0.49 Ry is taken for the s state of hydrogen. The charge augmentation pseudofunctions $Q_{ij}(\mathbf{r})$ have a cutoff radius $r_{inner} = 0.6$ a.u. for O and 0.5 a.u. for H, in such a way as to match the radial charge density and its first and second derivatives at r_{inner}, and to preserve the appropriate moments of the charge density, while maximizing the smoothness using a procedure[34] similar to that used by Rappe *et al.*[36] for wave functions. In these calculations, we did not implement the use of an L-dependent r_{inner} as discussed in Ref. 34.

In the solid-state calculations,[37] the electronic wave functions are expanded in a basis of plane waves with kinetic energy up to 20 Ry. Only the Γ point is used for the Brillouin-zone summations. The program is used in three modes of operation. We use the first-order dissipative dynamics on the electrons (steepest descents) to calculate ground-state energies for systems with given ionic configurations. In some cases, we use dissipative dynamics simultaneously on electron and ion degrees of freedom, in order to identify a local minimum in the configuration space. For the dynamical calculations, we use the Car-Parrinello approach, i.e., second-order Newtonian dynamics on both the fictitious electronic and real ionic degrees of freedom. In our calculations, we take 4.3 a.u. for the time step and 400 a.u. for the fictitious electron mass. The simulation is always started from zero ionic velocities after a steepest-descent quench of the electronic coordinates at the fixed starting configuration. Some details of the implementation, including expressions for the forces and details of the method for evolving the constraint matrix in the Newtonian dynamics, are given in Ref. 34 (but note that the multiple grid scheme discussed there has not been used in the present work).

In all cases, the Ceperley-Alder exchange-correlation energies and potentials are used for the LDA.[11] Most of

the calculations are carried out using gradient corrections (GC) in addition, specifically using the Becke[14] parametrization for the exchange and the Perdew formula[13] for the correlation. For consistency, all GC solid-state calculations utilize pseudopotentials that are consistently generated with the same GC scheme.

IV. RESULTS

A. Tests on simple systems

We study energy-minimizing structures for H_2O monomers and dimers. The lattice constant of the unit cell is 13.0 a.u. and only the Γ point is included in the Brillouin-zone summation. The water molecule in the monomer calculation is positioned symmetrically with respect to the body diagonal of the cell, and the two oxygens in the dimer calculation are aligned on the body diagonal. In Table I, we compare our theoretical results for the O–H bond length and H–O–H bond angle of the H_2O monomer, and the O–O distance of the dimer, with experiment. It is clear that gradient corrections make for a dramatic improvement in the dimer O–O distance, a quantity which reflects the description of the hydrogen bond. Similar results have been reported from calculations utilizing conventional pseudopotentials[9] and all-electron methods.[38] Moreover, the underestimation of the O–O bond length by LDA is also consistent with our calculations of the equation of state of ice phases, to be discussed in Sec. IV C 1. Therefore, except where noted, the gradient corrections have been adopted for all of the calculations reported below.

B. Phonon density of states of ice I_c

We carry out molecular-dynamics simulations of the motion of atoms in the crystal of ice I_c, and calculate the phonon density of states from the Fourier transform of the velocity autocorrelation function. Initially, we take a lattice constant of 12.0 a.u. from experiment at $-130\,°C$.[39] The structure of ice I_c for our calculations is shown in Fig. 1. We arrange the oxygen and hydrogen atoms in a geometric configuration corresponding to isolated water molecules sitting in the diamond-structure sites in a cubic supercell. Since the crystal lattice of ice I_c is orientationally disordered, we generate all possible orientational configurations of the eight molecules in the supercell which do not violate Pauling's ice rules.[16] There are four physically distinct orientational configurations in this eight-molecule unit cell, with degeneracy 6, 12, 24, and 48 and polarization $\langle 100 \rangle$,

$\langle \frac{1}{2}\frac{1}{2}0 \rangle$, $\langle 000 \rangle$, and $\langle \frac{1}{2}00 \rangle$, respectively. We choose one of the configurations with degeneracy 48 because it is the most disordered configuration among the four. After relaxing the atomic degrees of freedom, we find the minimum-energy atomic configurations. The O–H bond length and H–O–H bond angle are found to be 1.92 a.u. and 108.5°, which may be compared with 1.866 a.u. and 104.7° for an isolated water molecule (see Ref. 40 or Table I), respectively. Then, we add randomly assigned normal-mode components to the minimum-energy atomic configuration in conformity with a target temperature 100 K. We simulate the atomic dynamics in the crystal for a duration of 320 fsec. From the series of atomic positions as a function of time, we calculate the velocities $v_i(t)$, their Fourier transforms $v_i(\omega)$, and the power spectrum $|v_i(\omega)|^2$. As discussed in the appendix, the latter is directly related to the phonon density of states in the thermodynamic and long-time limits. (It has to be understood that runs of finite length will exhibit thermal fluctuations in the weights of peaks in the power spectrum.) In practice, the maximum entropy method[41] is used to extract the power spectrum, thus providing better resolution at low frequencies. The number of data is 3074 with sampling interval 0.104 fsec, and the number of poles is 700. The phonon "density of states" obtained in this way is shown in Fig. 3.

By decomposing this density of states into the contributions from the normal modes of a water molecule, we identify the groups of peaks as bands arising from O–H stretching modes, H–O–H bending modes, librational modes, and translational modes, in the order of decreasing frequency. The corresponding projected densities of states for H_2O and D_2O ice are shown in Fig. 3. The isotope shifts which are evident from a comparison of the H_2O and D_2O ice I_c results can easily be seen to agree with expectations. In H_2O ice, the O–H stretching modes contribute to the peak near 3100 cm^{-1} which is shifted to near 2250 cm^{-1} in D_2O ice. The factor $(\frac{1}{2})^{1/2}$ serves to check the identification because the frequency of a vibration is inversely proportional to the square root of the mass of the vibrating particle. The H–O–H bending modes and librational modes also show a factor of $(\frac{1}{2})^{1/2}$, while the translational modes show a factor of $(\frac{18}{20})^{1/2}$. The experimental data on the absorption spectrum[17-24] are compared with theory in Table II. The agreement with experiments is good.

Note that the contributions from the different normal modes of the water molecule are well separated, consistent with the expectation that the intermolecular interaction (i.e., the hydrogen bond) should be weak com-

TABLE I. Structural properties of H_2O monomer and dimer.

Structural parameter	LDA	LDA+GC	Experiment
Monomer			
O–H bond length (a.u.)	1.849	1.866	1.809
H–O–H bond angle (deg.)	103.3	104.7	104.5
Dimer			
O–O distance (a.u.)	5.10	5.50	5.63

TABLE II. Comparison between spectra from theoretical calculations and from infrared and Raman spectra of ice I_c.

Mode	H_2O (cm^{-1})		D_2O (cm^{-1})	
	Theory	Experiment	Theory	Experiment
O–H stretching	2768–3124	3083–3380	2040–2264	2283–2420
H–O–H bending	1528	1650±30	1140	1210±10
Libration	620–1024	500–1050	376–612	350–750
Translation	196–352	54–305	176–316	54–294

pared to covalent or ionic chemical bonds. However, the hydrogen bond is strong enough to shift the O–H stretch frequency of H_2O ice I_c significantly from that of an isolated H_2O molecule, roughly 3100 vs 3680 cm^{-1},[8] respectively. The hydrogen-bonding interaction must also be responsible for the large width of the stretching-mode bands which is notable in Fig. 3. This could be explained either as inhomogeneous broadening associated with the proton disorder of the ice crystal, or as a simple banding resulting from the intermolecular interactions. As discussed in the next paragraph, we believe it is predominantly the latter. However, for reasons that are not yet clear, these effects do not seem to broaden the librational bands significantly; their frequencies remain remarkably narrow and well defined.

We also calculate the phonon densities of states within LDA. Preparation of the system is the same, except that we simulate atomic motions in all of the four distinct ice-rule configurations and that the duration of the molecular-dynamics simulations is 437 fsec. (We em-

phasize that both calculations were carried out at the same experimental lattice constant.) In comparison to the calculations with gradient corrections, the phonon densities of states have almost the same features and frequencies. However, the frequency of the O–H stretching mode from the LDA calculations is a little lower. We present in Fig. 4 the results on H_2O and D_2O ice for the four physically distinct proton configurations. It is notable that the phonon densities of states of cubic ice do not depend strongly on the proton configurations which may influence the local field. In particular, the widths of the O–H stretching bands do not correlate strongly with the degree of proton disorder. Finally, the librational mode again has a narrow and well-defined frequency regardless of the proton configurations.

C. Hydrogen-bond symmetrization

1. Equation of state of ice X

We study the hydrogen-bond symmetrization with increasing pressure in low- and high-pressure phases of ice. First, we calculate the equation of state for ice X. Total
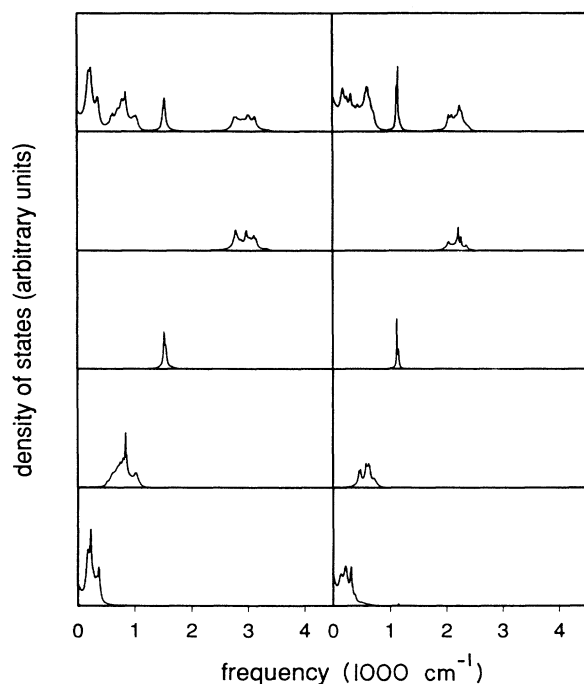

FIG. 3. Phonon densities of states of H_2O (left) and D_2O (right) ice I_c. From top to bottom; total, stretching, bending, librational, and transitional modes, respectively.
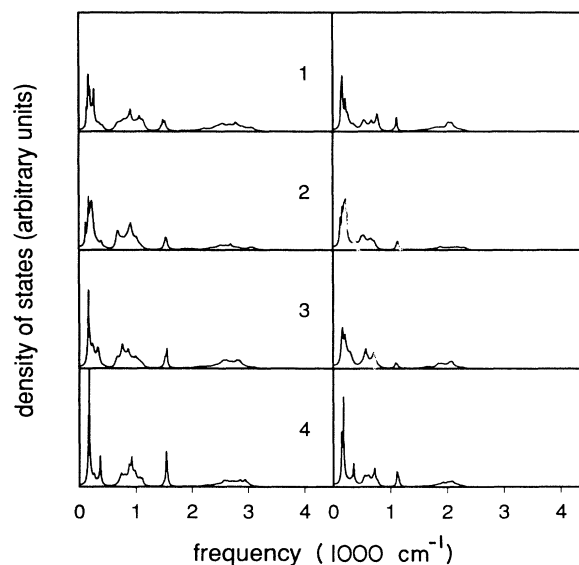

FIG. 4. Phonon densities of states of H_2O (left) and D_2O (right) ice I_c within LDA. The numbers 1, 2, 3, and 4 represent the proton configurations with polarization $\langle 100 \rangle$, $\langle \frac{1}{2}\frac{1}{2}0 \rangle$, $\langle 000 \rangle$, and $\langle \frac{1}{2}00 \rangle$, respectively.

TABLE III. Comparisons between theoretical and experimental equations of state of ice X.

Lattice constant (a.u.)	Pressure (GPa) from LDA	Pressure (GPa) from GC-LDA	Pressure (GPa) from experiment
9.9	13	103	114
10.0	8.3	97	97
10.1	3.2	91	87
10.2	−2.1	85	76
10.3	−7.5	78	71
10.4	−13	72	68
10.5	−19	65	61

energies are calculated at lattice constants from 10.0 to 12.0 a.u. in steps of 0.5 a.u., fixing all the protons in the unit cell at the bond midpoints, using both LDA and gradient-corrected LDA. The two sets of data points are fitted to quadratic functions as shown in Fig. 5. The hydrostatic pressure is calculated from the derivative of energy with respect to volume using the thermodynamic identity $p = -\partial E/\partial V$.[42] The equation of state from the calculations with the gradient-corrected LDA shows good agreement with the experimental equation of state of Hemley $et\ al.$[43] within a few percent error, while the equation of state from LDA alone underestimates the lattice constant at any given pressure by more than 10%. In fact, the pressure is $negative$ in the physically realizable range of lattice constants. The results are summarized in Table III and compared with experimental information. These results show that the gradient-corrected LDA is capable of giving a good description of the structural properties of H_2O ice, while the LDA description is severely inadequate.

2. Static energy calculations

We next investigate the stability of the ice X structure with respect to symmetry-breaking proton displacements.
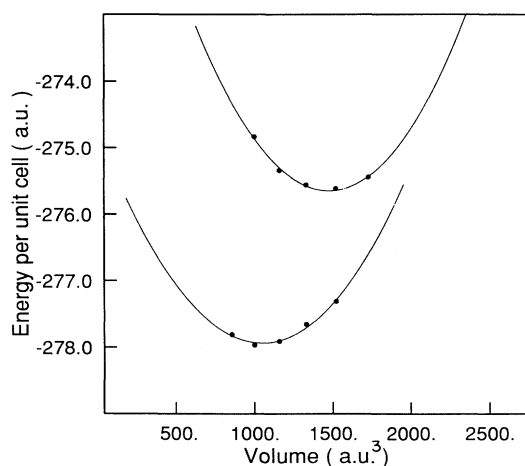

FIG. 5. Equation of state for ice X within LDA (left) and with gradient-corrected LDA (right). The dots are the calculated data and the curve is the fitted quadratic function.

We calculate the total energies of the unit cell with lattice constants 10.0, 10.5, and 11.0 a.u. as we displace all the protons away from the bond midpoints by the same amount δ in an antiferroelectric pattern, simulating the ice VIII structure, and fit the resulting data points to fourth-order polynomials. If the protons had infinite masses, the transition into the asymmetric positions would occur when the coefficient of the quadratic term changes its sign, since this is the point at which the potential-energy surface develops a double minimum. The coefficients of the quadratic terms are found to be approximately linear in lattice constant over the range of interest, crossing zero at about 9.9 a.u. This corresponds to 103 GPa in our theoretical equation of state, exceeding the experimental transition pressure by more than a factor of 2.

However, the protons are so light that their quantum fluctuations are not negligible. Based on the theory of Koehler and Gillis,[44] we estimate the size of the quantum fluctuation effects of the protons. In this theory, we consider a system of interacting quartic anharmonic oscillators whose Hamiltonian consists of an on-site term H_0 and an intercell coupling term H_1 which is treated in the mean-field approximation:

$$H_0 = -\frac{1}{2M}\frac{d^2}{du^2} + \frac{1}{2}\alpha u^2 + \varphi u^4 , \tag{1}$$

$$H_1 = -\chi u \langle u \rangle , \tag{2}$$

where M is the mass of the proton, u is the displacement from the bond midpoint, and atomic units are used. The mean-field approximation is expected to work fairly well here because the interaction between water molecules is a long-range dipole-dipole interaction. H_0 above describes the motion of a single proton, holding all other protons fixed, while the calculations of Fig. 6 correspond to thinking of u as an antiferroelectric collective coordinate; thus, in the classical mean-field limit we can identify $H_0 + H_1 = \frac{1}{2}(\alpha - \chi)u^2 + \varphi u^4$. The classical transition to the asymmetric structure would occur at $\chi - \alpha = 0$. When quantum fluctuation effects are considered by including the kinetic-energy term in H_0, we expect the transition to be shifted so that it will not occur until some positive value of $\chi - \alpha$. Using the variational technique,[44] one finds that the transition occurs if

$$\chi^{1/2}(\chi - \alpha) = 6\varphi/\sqrt{M} . \tag{3}$$

We find that this condition is satisfied at lattice constant 10.74 a.u., which corresponds to 49 GPa in our equation of state shown in Fig. 5. This is now in excellent agreement with the experimental estimates of 42 to 47.5 GPa.

We also estimate the effect of the proton quantum fluctuation on our theoretical equation of state, as this could also affect the predicted transition pressure. Since the oxygens are much heavier than protons, we assume their quantum fluctuation effects are negligible, and we treat the oxygen sublattice as rigid. We calculate the proton ground-state wave functions and energies in the fitted single-bond potential-energy curve, and add these

ground-state energies to the total DFT energies of the unit cell. It is found that the quantum fluctuations increase the pressure by only about 6 GPa in the region of interest. As this is a rather small correction, we have not considered it further.

We also calculated the transition lattice constants for other types of proton displacement patterns consistent with the Pauling ice rules, such as a ferroelectric pattern and a disordered pattern. We found no significant difference in the transition lattice constants regardless of the type of displacement. Moreover, at least within the mean-field theory outlined above, the shift in the transition point due to quantum fluctuations should be roughly the same for each. Therefore, our calculations do not predict which displacement pattern is favored. However, we think the antiferroelectric displacement pattern of ice VIII is likely to require the lowest energy when coupling of the proton distortions to the tetragonal strain is taken into account. Of course this advantage will be offset somewhat at higher temperatures, where the higher entropy of the ice VII will lower its free energy. We have not attempted a quantitative analysis of these competing effects.

3. Molecular-dynamics simulations

So far we have confirmed that our theory does give a transition near the experimentally observed one. In order to understand better the nature of the transition, we try to find a soft phonon mode at the transition by simulating the atomic vibrational dynamics. While the Car-Parrinello *ab initio* molecular dynamics assumes the validity of classical mechanics[10] and therefore neglects quantum fluctuation effects, this approach should still give important insight into the nature of the transition. We prepare the system in such a way that the ions in the unit cell deviate from the positions in ice X by a small amount in a random fashion and the electrons are in their ground state. We let the system evolve for a duration of about 250 fsec. The phonon density of states is calculat-

ed from the Fourier transform of the velocity autocorrelation function with the help of the maximum-entropy method, as before, and the total phonon density of states is again decomposed into the contributions from different normal modes of the system. In Fig. 7, we show the total phonon density of states and the density of states projected onto the stretching mode (SM) of the protons, for several different lattice constants. Note that as the lattice constant approaches the transition from below, the SM-projected density of states moves toward lower frequency. We further decompose the SM's of the protons into those that preserve the ice rules, and those that violate them. The densities of states of the ice-rule-preserving SM are shown in the right column of Fig. 7; clearly, therefore, the higher-frequency peaks in the middle column correspond to the ice-rule-violating SM's.

Our interpretation of Fig. 7 is that the ice-rule-preserving SM's go soft (i.e., ω^2 goes to zero) somewhere between 10.0 and 10.5 a.u. confirming the interpretation in terms of a mode-softening transition. The theory of the previous parts suggests it should go soft closer to 10.0 a.u.; the fact that it seems to go at a slightly higher lattice constant probably reflects anharmonic effects associated with thermal fluctuations in the molecular-dynamics simulations, which were done at low but nonzero temperature. We confirm this by finite temperature mean-field theory.[45] We investigate how much the transition lattice constant would change due to the finite temperature of the molecular-dynamics simulations. We measure the temperature of the simulations to be $T = 647$ and 569 K at 10.0 and 10.5 a.u., respectively. These temperatures are somewhat higher than the relevant experiments, which are done at 100 K (Ref. 28) and 300 K (Ref. 29), but we think they are not too high to be meaningful.
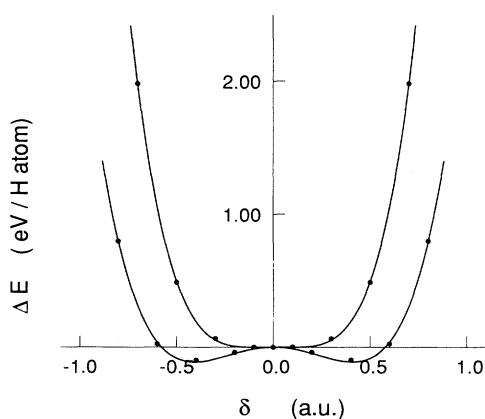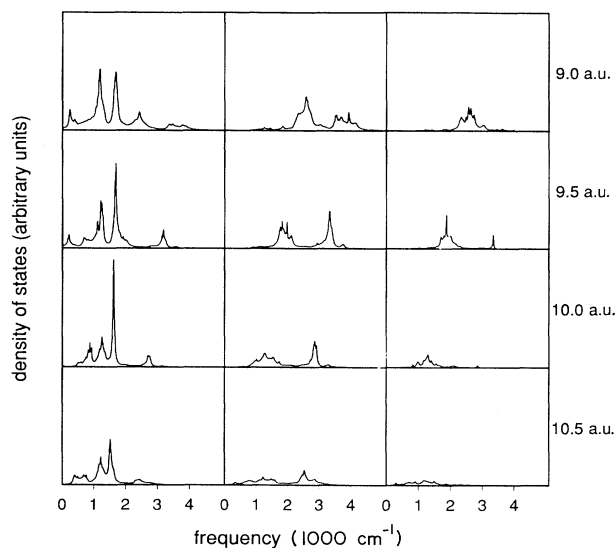

FIG. 6. Born-Oppenheimer potential-energy surfaces of an antiferroelectric collective mode in the ice-X structure. The upper and lower curves correspond to lattice constants of 10.0 and 11.0 a.u., respectively.

FIG. 7. Total densities of states of ice X at several lattice constants (left), and the densities of states projected onto all O–H stretching modes (middle), and only ice-rule preserving stretching modes (right) of the protons. Vertical axis is scaled by a factor of 2.4 in middle and right panels.

Even in the classical case, the expectation value of the proton displacement from the bond midpoint $\langle u^2 \rangle$ does not become nonzero when the potential develops a double minimum. The critical temperature and the critical intercell coupling χ are related as follows, again from simple mean-field theory:

$$k_B T = \chi \langle u^2 \rangle , \qquad (4)$$

where

$$\langle u^2 \rangle = \frac{\int u^2 \exp[-V(u)/k_B T]du}{\int \exp[-V(u)/k_B T]du} , \qquad (5)$$

and

$$V(u) = \tfrac{1}{2}\alpha u^2 + \phi u^4 . \qquad (6)$$

Calculating $\langle u^2 \rangle$ numerically at the temperature of the molecular-dynamics simulations, we get the critical χ. Comparing the critical χ to the actual χ, we find that it is in the symmetric regime at 10.0 a.u. (i.e., actual χ is smaller than the critical χ) and in the asymmetric regime at 10.5 a.u. (i.e., actual χ is larger than the critical χ). So, the classical transition at finite temperature should be between 10.0 and 10.5 a.u. It is difficult to predict the transition lattice constant with confidence, but assuming that the actual and critical χ can be smoothly interpolated over the range of lattice constants between 10.0 and 10.5 a.u., we estimate that the transition should occur at about 10.37 a.u. Therefore we think the finite temperature is responsible for the discrepancy between static and dynamic estimates of the location of the classical transition.

4. Hydrogen-bond symmetrization in ice I_c

We have thus far studied the hydrogen-bond symmetrization in the high-pressure phases ice VII-VIII. There has been a prediction that the hydrogen bond in the low-pressure cubic ice phase should also become symmetrized, but at a much lower pressure.[32] Here, we carry over our previous analysis to the case of ice I_c, calculating the equation of state and attempting to predict the critical pressure for the transition into symmetrically hydrogen-bonded cubic ice. We use the ice I_c supercell having the most disordered proton configuration, with polarization $\langle \tfrac{1}{2}00 \rangle$. The total energies of the unit cell are calculated with gradient-corrected LDA at lattice constants from 10.0 to 12.0 a.u. in steps of 0.5 a.u., allowing the atomic configurations to relax at each lattice constant. The calculations were also repeated for the symmetric structure, in which the protons are fixed at the O–O "bond" midpoints, and the O atoms lying on a diamond lattice. The data points and the fitted function are shown in Fig. 8. The equilibrium lattice constants for the two structures are found to be 11.58 a.u. for ice I_c and 11.01 a.u. for symmetrically hydrogen-bonded cubic ice, respectively. (However, the latter figure has limited significance, as the symmetric phase is unstable to the I_c phase except at zero pressure.) The calculated equilibri-

um volume of 11.58 a.u. for ice I_c is about 3% less than the experimental value of 12.0 a.u. adopted in Sec. IV B for the phonon calculations. However, this small discrepancy would most likely be reduced further if the effect of the H quantum fluctuations on the equation of state were considered, as discussed above in Sec. IV C 1.

The hydrostatic pressure is calculated from the equation of state in the same way as for ice X, and the same mean-field analysis of the collective and single-bond H potentials is carried out. We find that the transition between ice I_c and symmetrically hydrogen-bonded cubic ice occurs at a lattice constant is 10.80 a.u., which corresponds to 7 GPa using our calculated equation of state. This is well above the pressure of about 0.213 GPa at which ice I_h transforms into other denser phases such as ice II or ice III at $-35\,°\mathrm{C}$,[15] and ice I_c is metastable with respect to ice I_h at lower pressure. (The rather low transition pressure out of ice I_c and I_h can easily be understood because these phases are characterized by a large amount of empty space in the crystal structure.) Thus, it is not surprising that symmetric hydrogen-bonded cubic ice has not been observed experimentally.

V. CONCLUSION

We have presented results from a study of the structural and dynamical properties of various phases of ice carried out using the *ab initio* molecular-dynamics method combined with ultrasoft pseudopotentials. We have found that the LDA must be augmented with gradient corrections for a proper description of the hydrogen bonding. The phonon density of states of cubic ice has been extracted from the molecular-dynamics simulations. We have calculated the equations of states for ice I_c, symmetrically hydrogen-bonded cubic ice, and the ice VII-VIII-X system. We have also calculated the critical pressure of the transition into the symmetrically hydrogen-bonded phases. The transition from ice VIII-
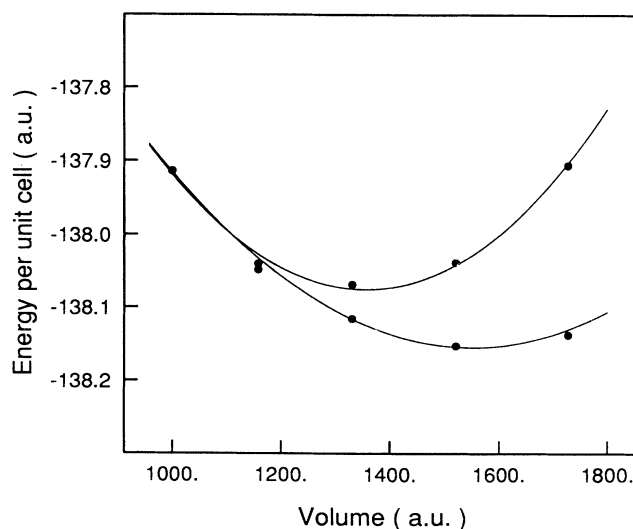

FIG. 8. Equations of state for ice I_c and symmetrically hydrogen-bonded cubic ice. The dots are calculated data and the curves are the fitted quadratic functions.

VII to ice X is predicted to occur at about 49 GPa when the effects of the quantum fluctuations of the protons are included within mean-field theory. While the peaks in the phonon density of states corresponding to most other modes shift only moderately lower in frequency with increasing pressure, the modes corresponding to O–H stretch combinations which preserve the ice rules becomes soft ($\omega^2 \to 0$) at the transition. The phase transition between ice I_c and symmetric hydrogen-bonded cubic ice is predicted to occur at 7 GPa. The theoretical results are in good agreement with experiments.

This work also helps to demonstrate the accuracy and efficiency of calculations using the recently introduced ultrasoft pseudopotentials. Calculations on a rather complex system containing oxygen atoms were carried out at modest computational cost. We hope this calculational scheme will provide many future opportunities to carry out first-principles calculations of the structural and electronic properties of materials that include first-row and transition-metal elements. Other properties of ice, such as the ionic and orientational defects in ice crystals,[46] the hydration geometry around an anion (CI^-, etc.) or a cation (Ni^{2+}, Ca^{2+}, Mn^{2+}, etc.),[47,48] and the structural and dynamical properties of bulk water,[49–55] are interesting problems which are now open to treatment using similar methods. Studies of transition-metal systems are also coming within reach, as evidenced by a recent calculation on liquid Cu by Pasquarello *et al.*[56] Thus, the approach used here should be very useful in future studies of a wide range of systems that have previously been difficult to study using plane-wave-based DFT methods.

APPENDIX: DENSITY OF STATES FROM VELOCITY AUTOCORRELATION FUNCTION

We discuss how the Fourier transform of the velocity autocorrelation function is related to the phonon density of states. The immediate output from the molecular-dynamics simulations is the time trace $v(t_k)$ with $k = 1, \ldots, N$. According to the definition of the density of states, we are required to count frequencies which are equal to ω:

$$g(\omega) = \sum_{jk} \delta(\omega - \omega_j(\mathbf{k})) \ . \tag{A1}$$

Using second quantized notation, the αth Cartesian component of the velocity of the κth atom in the lth unit cell, $v_{\alpha l \kappa}(t)$, is given by

$$v_{\alpha l \kappa}(t) = \left[\frac{\hbar}{\mathcal{N} M_\kappa} \right]^{1/2} \sum_{jk} e^j_{\alpha \kappa}(\mathbf{k})[-i\omega_j(\mathbf{k})]\exp[-i\omega_j(\mathbf{k})t + i\mathbf{k}\cdot\mathbf{R}_l] \left[\frac{1}{2\omega_j(\mathbf{k})} \right]^{1/2} [a_j(\mathbf{k}) + a_j^\dagger(-\mathbf{k})] \ , \tag{A2}$$

where $e^j_{\alpha\kappa}(\mathbf{k})$ is the polarization vector, $\mathcal{N}$ is the number of atoms, M_κ is the mass of κth atom, and $a_j(\mathbf{k})$, $a_j^\dagger(\mathbf{k})$ are the annihilation and creation operators. Using the commutation relations between the annihilation and creation operators,

$$[a_j(\mathbf{k}), a_{j'}^\dagger(\mathbf{k}')] = \delta_{jj'}\delta(\mathbf{k}-\mathbf{k}') \ , \tag{A3}$$

$$[a_j(\mathbf{k}), a_{j'}(\mathbf{k}')] = [a_j^\dagger(\mathbf{k}), a_{j'}^\dagger(\mathbf{k}')] = 0 \ , \tag{A4}$$

it follows that

$$\sum_{\alpha l \kappa} M_\kappa \langle v_{\alpha l \kappa}(t) v_{\alpha l \kappa}(0) \rangle = -\frac{(2\pi)^3}{V} \sum_{jk} \exp[-i\omega_j(\mathbf{k})t]\langle \hbar\omega_j(\mathbf{k})[n_j(\mathbf{k}) + \tfrac{1}{2}] \rangle \ . \tag{A5}$$

In the thermodynamic limit, the quantity in the bracket in the right-hand side is $k_B T$. (This does not necessarily mean that the energy in each mode is equal in a finite run, as in Figs. 3 or 4.) By taking the Fourier transform of both sides of Eq. (A5), it follows that

$$\sum_{\alpha l \kappa} M_\kappa \langle |v_{\alpha l \kappa}(\omega)|^2 \rangle = -\frac{(2\pi)^3}{V} k_B T \sum_{jk} \delta(\omega - \omega_j(\mathbf{k})) \ , \tag{A6}$$

where the left-hand side is the density of states within a constant factor.

*Present address: Laboratory of Atomic and Solid State Physics, Cornell University, Ithaca, New York 14853-2501.

†Present address: IBM Research Division, Zürich Research Laboratory, CH-8803 Rüschlikon, Switzerland.

[1]J. Del Bene and J. A. Pople, Chem. Phys. Lett. **4**, 426 (1969).

[2]K. Morokuma and J. R. Winick, J. Chem. Phys. **52**, 1301 (1970).

[3]M. J. Firsh, J. E. Del Bene, J. S. Binkley, and H. F. Schaefer III, J. Chem. Phys. **84**, 2279 (1986).

[4]B. J. Smith, D. J. Swanton, J. A. Pople, H. F. Schaefer III, and L. Radom, J. Chem. Phys. **92**, 1240 (1990).

[5]J. Del Bene and J. A. Pople, J. Chem. Phys. **52**, 4858 (1970).

[6]R. Knochenmuss and S. Leutwyler, J. Chem. Phys. **96**, 5233 (1992).

[7]W. Kohn and L. J. Sham, Phys. Rev. **140**, A1133 (1965).

[8]J. E. Müller, R. O. Jones, and J. Harris, J. Chem. Phys. **79**, 1874 (1983).

[9]K. Laasonen, F. Csajka, and M. Parrinello, Chem. Phys. Lett. **194**, 172 (1992).

[10]R. Car and M. Parrinello, Phys. Rev. Lett. **55**, 2471 (1985).

[11]D. M. Ceperley and B. J. Alder, Phys. Rev. Lett. **45**, 566 (1980); D. Ceperley, Phys. Rev. B **18**, 3126 (1978).

[12]D. Vanderbilt, Phys. Rev. B **41**, 7892 (1990).

[13]J. P. Perdew, Phys. Rev. B **33**, 8822 (1986).

[14]A. D. Becke, Phys. Rev. A **38**, 3098 (1988).

[15]P. V. Hobbs, *Ice Physics* (Clarendon, Oxford, 1974).

[16]L. Pauling, Proc. Nat. Acad. Sci. USA **14**, 359 (1928).

[17]N. Ockman, Adv. Phys. **7**, 199 (1958).

[18]J. E. Bertie and S. M. Jacobs, J. Chem. Phys. **67**, 2445 (1977).

[19]J. E. Bertie and E. Whalley, J. Chem. Phys. **40**, 1637 (1964).

[20]J. E. Bertie and E. Whalley, J. Chem. Phys. **46**, 1271 (1967).

[21]R. Zimmermann and G. C. Pimentel, in *Advances in Molecular Spectroscopy*, edited by A. Mangini (Macmillan, New York, 1962), p. 762.

[22]J. R. Scherer and R. G. Snyder, J. Chem. Phys. **67**, 4794 (1977).

[23]M. J. Taylor and E. Whalley, J. Chem. Phys. **40**, 1660 (1964).

[24]P. T. T. Wong and E. Whalley, J. Chem. Phys. **65**, 829 (1976).

[25]M. Marchi, J. S. Tse, and M. L. Klein, J. Chem. Soc. Faraday Trans. 2 **83**, 1867 (1987).

[26]M. S. Bergren and S. A. Rice, J. Chem. Phys. **77**, 583 (1982).

[27]G. C. Pimentel and A. L. McClellan, *The Hydrond Bond* (Freeman, San Francisco, 1960), p. 259.

[28]K. R. Hirsch and W. B. Holzapfel, J. Chem. Phys. **84**, 2771 (1986).

[29]A. Polian and M. Grimsditch, Phys. Rev. Lett. **52**, 1312 (1984).

[30]G. E. Walrafen, M. Abebe, F. A. Mauer, S. Block, G. J. Piermarini, and R. Munro, J. Chem. Phys. **77**, 2166 (1982).

[31]W. B. Holzapfel, J. Chem. Phys. **56**, 712 (1972).

[32]F. H. Stillinger and K. S. Schweizer, J. Phys. Chem. **87**, 4281 (1983).

[33]K. S. Schweizer and F. H. Stillinger, J. Chem. Phys. **80**, 1230 (1984).

[34]K. Laasonen, A. Pasquarello, C. Lee, R. Car, and D. Vanderbilt (unpublished).

[35]K. Laasonen, R. Car, C. Lee, and D. Vanderbilt, Phys. Rev. B **43**, 6796 (1991).

[36]A. M. Rappe, K. M. Rabe, E. Kaxiras, and J. D. Joannopoulos, Phys. Rev. B **41**, 1227 (1990).

[37]C. Lee, D. Vanderbilt, K. Laasonen, R. Car, and M. Parrinello, Phys. Rev. Lett. **69**, 462 (1992).

[38]J. Andzelm and E. Wimmer (unpublished).

[39]M. Blackman and N. D. Lisgarten, Adv. Phys. **7**, 189 (1958).

[40]K. Laasonen, R. Car, M. Parrinello, C. Lee, and D. Vanderbilt (unpublished).

[41]W. H. Press, B. P. Flannery, S. A. Teukolsky, and W. T. Vetterling, *Numerical Recipes* (Cambridge University Press, Cambridge, 1989), p. 430.

[42]M. T. Yin and Marvin L. Cohen, Phys. Rev. B **26**, 5668 (1982).

[43]R. J. Hemley, A. P. Jephcoat, H. K. Mao, C. S. Zha, L. W. Finger, and D. E. Cox, Nature **330**, 737 (1987).

[44]T. R. Koehler and N. S. Gillis, Phys. Rev. B **7**, 4980 (1973).

[45]M. E. Lines and A. M. Glass, *Principles and Applications of Ferroelectrics and Related Materials* (Clarendon, Oxford, 1977), p. 24.

[46]N. H. Fletcher, *The Chemical Physics of Ice* (Cambridge University Press, London, 1970), Chap. 7.

[47]F. Franks, in *Water, A Comprehensive Treatise* (Plenum, New York, 1972), Vol. 6, Chap. 1.

[48]K. Ramani Lata, N. Sahoo, and T. P. Das, J. Chem. Phys. **94**, 3715 (1991).

[49]W. L. Jorgensen, J. Chandrasekhar, J. D. Madura, R. W. Impey, and M. L. Klein, J. Chem. Phys. **79**, 926 (1983).

[50]W. L. Jorgensen and J. D. Madura, Mol. Phys. **56**, 1381 (1985).

[51]M. Mezei and D. L. Beveridge, J. Chem. Phys. **74**, 622 (1981).

[52]R. D. Mountain, J. Chem. Phys. **90**, 1866 (1989).

[53]M. Neumann, J. Chem. Phys. **85**, 1567 (1986).

[54]H. Tanaka and I. Ohmine, J. Chem. Phys. **87**, 6128 (1987).

[55]D. C. Rapaport, Mol. Phys. **50**, 1151 (1983).

[56]A. Pasquarello, K. Laasonen, R. Car, C. Lee, and D. Vanderbilt, Phys. Rev. Lett. **69**, 1982 (1992).